



# Manufacture and characteristics of Al<sub>2</sub>O<sub>3</sub> composite coating on steel substrate by SHS process

Hai-Dong Gao, Ze-Hua Wang\* , Jia Shao

Received: 12 October 2016/Revised: 10 January 2017/Accepted: 4 October 2017/Published online: 29 October 2017  
© The Nonferrous Metals Society of China and Springer-Verlag GmbH Germany 2017

**Abstract** Many steel components are needed to be reinforced on their surface to have a high abrasive resistance and corrosion resistance. Based on self-propagating high-temperature synthesis, a process to making Al<sub>2</sub>O<sub>3</sub> composite coatings on mild steel substrate in atmospheric environment with the help of simple auxiliary facilities was developed successfully. A pre-coated bilayer coating was employed. The effects of Fe content in pre-coated transition layer on phase composition, porosity and interfacial bonding were studied using scanning electron microscopy (SEM), energy-dispersive spectrum (EDS) and X-ray diffraction (XRD). The thermal shock resistance and abrasive resistance were investigated. When Fe content changes from 0 wt% to 50 wt%, the bond quality at first becomes better and then worse gradually. When Fe content is less 20 wt%, there is a small gap between the transition layer and the substrate; when Fe contents are 30 wt% and 40 wt%, working layer, the transition layer and the substrate bond together well. The working layer is mainly composed of Al<sub>2</sub>O<sub>3</sub>, Fe–Cr and Al(Cr)<sub>2</sub>O<sub>3</sub> phases and has a dense structure with porosity of less than 1%. The coating has a good thermal shock resistance and abrasive resistance. The abrasive resistance of the working layer is about ten times that of the substrate.

**Keywords** Al<sub>2</sub>O<sub>3</sub> composite coating; Self-propagating high-temperature synthesis; Interfacial bonding; Thermal shock resistance; Abrasive resistance

## 1 Introduction

Abrasion starts at the surface of the material. Improving the abrasive resistance of the surface is an effective way to prolong the service life of the mechanical parts [1, 2]. Al<sub>2</sub>O<sub>3</sub> composite coatings have an attractive interest due to its elevated hardness value and high abrasive resistance [3–5]. Many researchers attempted to fabricate Al<sub>2</sub>O<sub>3</sub> coatings on metal substrates using modern techniques, such as laser cladding [6, 7], atmospheric plasma spraying [8, 9], sol–gel method [10, 11], etc. However, these techniques are complex and expensive, or not suitable to produce a thick abrasive coating. Self-propagating high-temperature synthesis (SHS) is a potential method for the preparation of high performance Al<sub>2</sub>O<sub>3</sub> coating [12, 13]. Combining with centrifugal casting technology, SHS is successfully used to produce a ceramic coating on internal surface of steel tubes [14–16]. But how to manufacture a ceramic coating on a flat substrate using SHS technology is still a question [17]. Generally, high reaction temperature may result in a good interface binding. On the contrary, low reaction temperature may result in a smooth coating, but a bad interface binding. The interface bond quality conflicts with coating morphology on requirement of the reaction temperature. Previous research showed that the reaction can be changed using different additives in the SHS reaction system [18, 19]. Attempts were made to investigate the effect of Fe on the characteristics of coating, such as phase composition, content of porosity, interface bonding, thermal shock resistance and abrasive resistance.

H.-D. Gao, Z.-H. Wang\*, J. Shao  
College of Mechanics and Materials, Hohai University,  
Nanjing 210098, China  
e-mail: zhwang@hhu.edu.cn

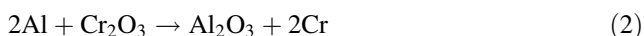
## 2 Experimental

### 2.1 Materials

Aluminum powder, graphite powder, titanium powder, nickel powder, ferric oxide powder, chromium oxide powder and iron powder were used in the experiment. The grain size and the purity of starting powders are shown in Table 1. Mild steel Q235 was used as substrate, and its chemical composition is shown in Table 2. Surface of the substrate was sandblasted for removing oxide.

### 2.2 Fabrication of coating

Pre-coated bilayer coating was designed, as shown in Fig. 1. Al–Fe<sub>2</sub>O<sub>3</sub>–Cr<sub>2</sub>O<sub>3</sub> system was selected as pre-coated working layer. The molar ratio of the Al–Fe<sub>2</sub>O<sub>3</sub>–Cr<sub>2</sub>O<sub>3</sub> system is determined, based on Reactions (1) and (2) mainly. Because aluminum powder is very active and easy to be oxidized, a little more aluminum powder was added. So Fe<sub>2</sub>O<sub>3</sub>:Cr<sub>2</sub>O<sub>3</sub>:Al was controlled at molar ratio of 6:4:21. Titanium powder and graphite powder were used in pre-coated transition layer. The wetting angle between Al<sub>2</sub>O<sub>3</sub> and Q235 steel is 141° (*T* = 1823 K), which means that they are difficult to bind together. While the wetting angles between TiC and Fe, TiC and Al<sub>2</sub>O<sub>3</sub> are both less than 90°, meaning that TiC could bind both Fe and Al<sub>2</sub>O<sub>3</sub> easily. Based on this reason, TiC was selected as a transition material between Al<sub>2</sub>O<sub>3</sub> ceramic coating and steel substrate. Titanium powder and graphite powder were added at molar ratio of 1:1 according to Reaction (3). In order to adjust the reaction intensity of SHS process, certain amount of Fe powders and Ni powders were added in the pre-coated transition layer, as shown in Table 3.



Different kinds of powders were mixed homogeneously in a self-made mixer for 6 h. The mixture of the powders was brushed to the blasted steel substrate. The transition layer is 3 mm in thickness, and the working layer is 22 mm in thickness. The pre-coated sample was placed in an

**Table 1** Purity of powders used in this experiment

Powder	Al	C	Ti	Ni	Fe <sub>2</sub> O <sub>3</sub>	Cr <sub>2</sub> O <sub>3</sub>	Fe
Grain size/ μm	4–70	≤ 30	44	50–75	0.2–0.8	0.5–2.0	130
Purity/wt%	99.0	99.0	99.5	95.0	99.0	99.0	99.0

**Table 2** Chemical composition of Q235 steel (wt%)

C	Si	Mn	P	S	Fe
0.140–0.220	≤ 0.300	0.300–0.650	≤ 0.045	≤ 0.050	Bal.

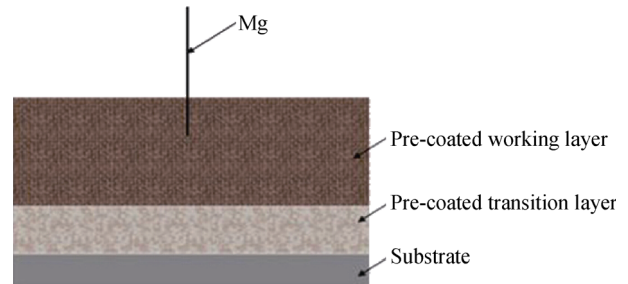


**Fig. 1** Schematic of bilayered structure coating

**Table 3** Ti + C, Ni and Fe contents of transition layer (wt%)

Samples	Ti + C	Ni	Fe
Coating 0	95	5	0
Coating 1	85	5	10
Coating 2	75	5	20
Coating 3	65	5	30
Coating 4	55	5	40
Coating 5	45	5	50

electrical resistance furnace, holding at 500 °C for 15 min, and then it was ignited using magnesium ribbon. Figure 2 shows the specific process of coating preparation.

### 2.3 Characterizations

The microstructure and interfacial bonding of the coating were observed by scanning electron microscope (SEM, Hitachi S-3400N). The chemical elemental distribution was measured using energy-dispersive spectrum (EDS, Horiba EX-250). The phase composition was analyzed using X-ray diffractometer (XRD, Bruker D8-ADVANCE). The porosity was determined using TD2000 image analysis software. The hardness of the coating was measured using HXD-1000TC Vickers microhardness tester. The hardness distribution vertical to the interface was tested on the cross section at an interval of 1/7 coating thickness.

Thermal shock test was conducted according to H8304-2007 JIS. The coated sample was heated to 800 °C in an electric furnace and held for 5 min and then dipped into water at room temperature for quick cooling. The numbers of this process can be used not only to characterize the

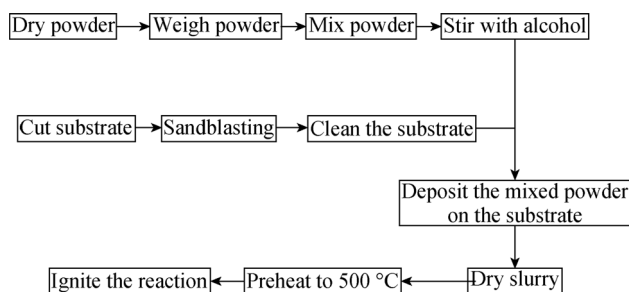


**Fig. 2** The process of fabricating composite coating

thermal shock resistance of the coating, but also to determine the bonding quality of the coating.

The abrasive test was carried out using WLS-225 tribometer, as shown in Fig. 3. The testing parameters are listed in Table 4. Quartz sand was added into water in a mass ratio of 1.5:1 as mortar materials. The wear rate was calculated by the formula  $W = M/PS$ , where  $W$  represents the wear rate,  $M$  indicates the mass loss of the sample,  $S$  means the total sliding distance, and  $P$  is the applied load [20–22]. The samples were weighed using an electronic scale with accuracy of 0.1 mg.

### 3 Results and discussion

#### 3.1 Effect of Fe on interfacial bonding

##### 3.1.1 Interface between substrate and transition layer

Figure 4 exhibits cross-sectional SEM images of interfacial bonding between substrate and transition layer when Fe content of pre-coated layer changes from 0 wt% to 50 wt%. When Fe addition increases from 0 wt% to 30 wt%, gas holes and the gap between the transition layer and substrate become smaller and smaller gradually. With Fe addition increasing to 30 wt% and 40 wt%, the coatings are the best. The transition layer and substrate bond well, and there are a small amount of gas holes in the coating. When 50 wt% Fe is added to the pre-coated layer, a big

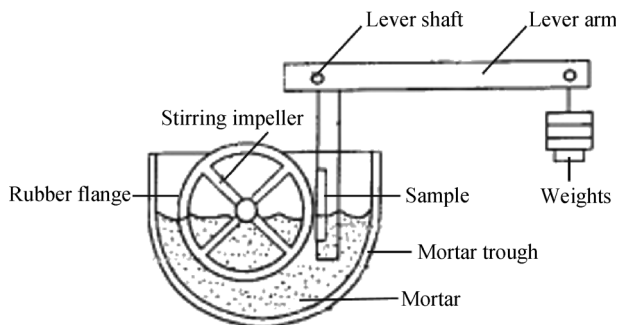


**Fig. 3** Schematic diagram of WLS-225 tribometer

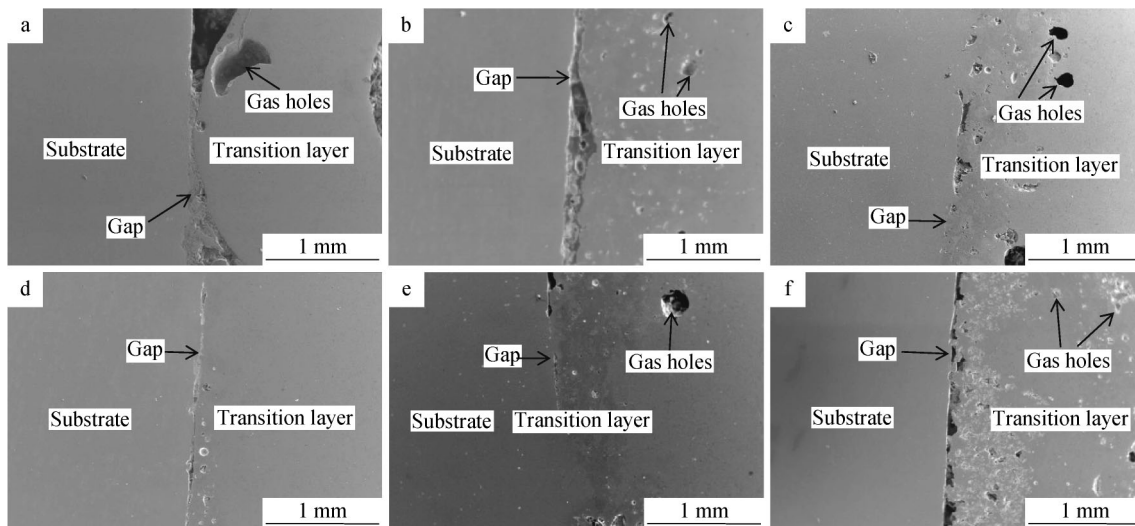
**Table 4** Abrasive testing parameters

Diameter of rubber wheel/mm	178
Rotational speed/(r·min <sup>-1</sup> )	240
Load/N	50
Wear time/min	30
Quartz sand/μm	38–45

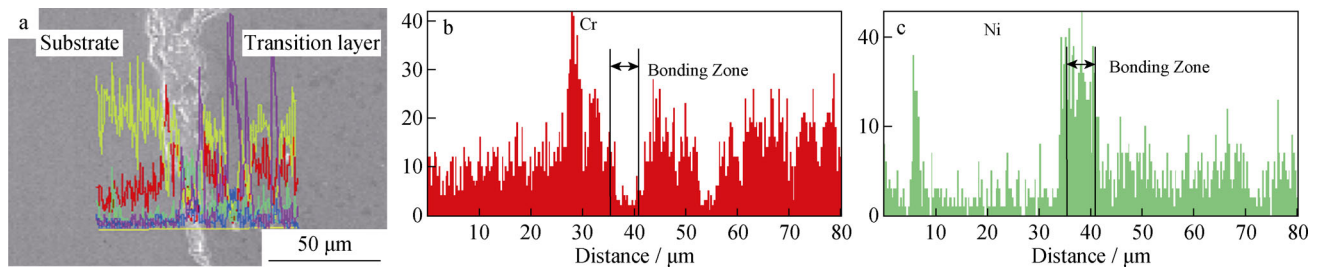
gap between the transition layer and substrate will appear. Figure 4a shows large pores in the transition layer and gaps at the interface when no Fe is added to the pre-coated layer. The cause may be considered that the reaction temperature is too high to make low melting point materials evaporated. When the gas does not escape during the solidification, gas holes will be formed in the coating. Meanwhile, liquid metal splashes and cools quickly. As a result, the gap between substrate and transition layer is lack of liquid metal to be filled. When adding 10 wt% Fe to the pre-coated layer, the reaction temperature is reduced a bit, but it is still very high. Gas holes and gaps still exist in the coating, as shown in Fig. 4b.

Figure 4c, d shows the interface between substrate and transition layer when Fe content of pre-coated layer changes from 20 wt% to 40 wt%. With the increase in Fe addition to the pre-coated transition layer, more heat is needed to melt Fe powders. Meanwhile, the content of Ti and C powders decreases correspondingly and the heat released from the reaction is reduced. So with the increase of Fe addition, the reaction temperature will be reduced and the reaction intensity can be alleviated. Less gas holes and less splashing will be formed. The transition layer and substrate can bind together well if the reaction temperature is high enough. If excessive Fe powders are added to the pre-coated materials, the reaction temperature is reduced too much, the surface layer of the substrate will not be melted. A profile of the surface will be remained. The substrate can not bond the coating metallurgically. Figure 4f shows bonding interface area when 50 wt% Fe was added to the pre-coated layer, which is a weak interfacial bonding.

A distribution of some chemical elements was analyzed by EDS. Figure 5 shows EDS analysis result of the coating with 30 wt% Fe to the pre-coated layer. It can be seen that there are high peaks of Ni and Cr on the side of mild steel substrate. It means that some of Ni and Cr diffuse into the substrate from the coating. Additionally, Fig. 4c–e shows that some areas between transition layer and substrate are bonded closely. Therefore, it can be considered that there is some metallic bonding between substrate and transition layer.



**Fig. 4** SEM images of interfacial bonding between substrate and transition layer: **a** 0% Fe, **b** 10% Fe, **c** 20% Fe, **d** 30% Fe, **e** 40% Fe, and **f** 50% Fe



**Fig. 5** **a** SEM image and EDS analysis (**b** Cr and **c** Ni) at interface area of substrate and transition layer

### 3.1.2 Interface between transition layer and working layer

Figure 6 exhibits the cross section of interface between transition layer and working layer when Fe content of pre-coated layer changes from 0 wt% to 50 wt%. Figure 6a shows SEM image of the coating without Fe addition to the pre-coated layer. It can be seen that there is not a clear profile of the interface between the working layer and the transition layer, but there are a big crack and holes in the working layer. Figure 6b shows SEM image of the coating added 10 wt% Fe to the pre-coated layer. Like Fig. 6a, there is not a clear profile of the interface between the working layer and the transition layer, but there are some holes in the transition layer. Figure 6c, d shows SEM images of the coating added 20 wt% and 30 wt% Fe to the pre-coated layer. Like Fig. 6b, there is not a clear profile of the interface between the working layer and the transition layer. Just some small holes exist in the working layer. When 40 wt% Fe is added to the pre-coated layer, the transition layer and the working layer bonds together tightly. But the profile of the interface becomes clear, as shown in Fig. 6e. When 50 wt% Fe is added to the pre-coated layer, the transition layer and the working layer do

not bond perfectly. Some cracks present at the interface between the transition layer and the working layer, as shown in Fig. 6f.

It can be concluded when Fe content is lower than 40 wt%, the transition layer and the working layer bond together well. Excessive Fe addition will deteriorate the binding quality. With the increase in Fe content, the number of holes reduces gradually. As a result, when 30 wt%–40 wt% Fe is added to the pre-coated layer, the transition layer and the working layer bond well and a dense coating is obtained. The reasons of Fe addition influencing the interface bonding between the transition layer and working layer are considered the same as to those of Fe addition influencing the interface between the substrate and the transition layer.

### 3.2 Microhardness of coating

Figure 7 shows the microhardness distribution across the section of the coatings. The microhardness of the substrate is low about HV<sub>0.3</sub> 224. Transition layer has a higher hardness than the substrate. Working layer has an extremely high hardness from HV<sub>0.3</sub> 1651 to HV<sub>0.3</sub> 2126. There

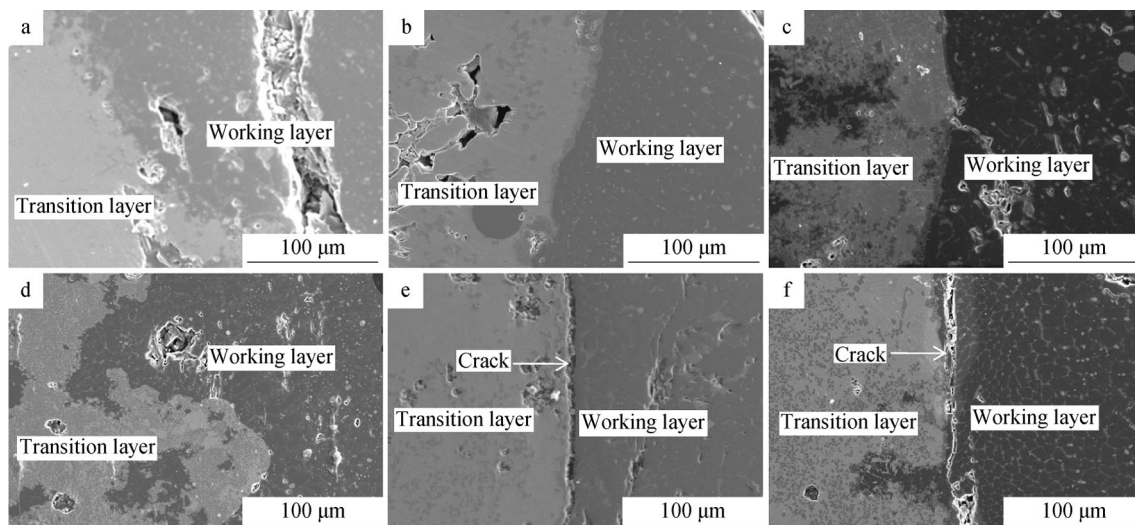


**Fig. 6** SEM images of interfacial bonding between transition layer and working layer: **a** 0% Fe, **b** 10% Fe, **c** 20% Fe, **d** 30% Fe, **e** 40% Fe, and **f** 50% Fe

are jumps at the interface. According to the analysis later, many TiC particles are produced in the transition layer and large numbers of  $\text{Al}_2\text{O}_3$  particles in the working layer. TiC particles are mostly less than  $2\ \mu\text{m}$  in size and play a role of dispersion strengthening in the transition layer. No doubt, TiC particles and  $\text{Al}_2\text{O}_3$  particles greatly improve the hardness of the transition layer and working layer, respectively [23, 24].

Another phenomenon is that with the increase in the distance from the interface between substrate and transition layer, the grain size of TiC particles increases, but the number decreases. It may cause a slight downward of the hardness. As for the coatings 2 and 3, due to that some  $\text{Al}_2\text{O}_3$  particles mix to the transition layer near the working layer, the hardness increases greatly.

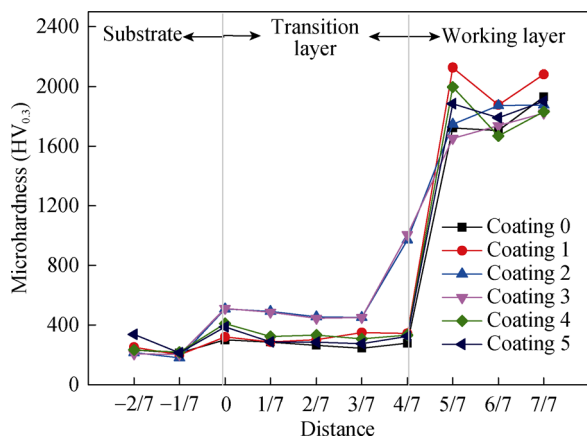


**Fig. 7** Hardness distribution across section of coatings

### 3.3 Thermal shock resistance of coating

Figure 8 shows the test result of the thermal shock resistance of the coating. With the increase in Fe addition, the thermal shock resistance exhibits a rising tendency at first and then downward. Figure 9 shows the crack propagation in coating 0 during thermal shock testing after 3, 7 and 15 cycles. With the increase in the number of thermal shock cycles, cracks propagate and new cracks initiate meanwhile. Cracks cross each other. Finally, a part of ceramic coating peels off the substrate. As known, different materials and different phases have different thermal expansion coefficient. When coatings of  $800\ ^\circ\text{C}$  are dipped into water, the ceramic coating and steel substrate will produce different contractions. A significant thermal stress will be resulted especially in an area between the coating and the substrate. This thermal stress can undoubtedly initiate the

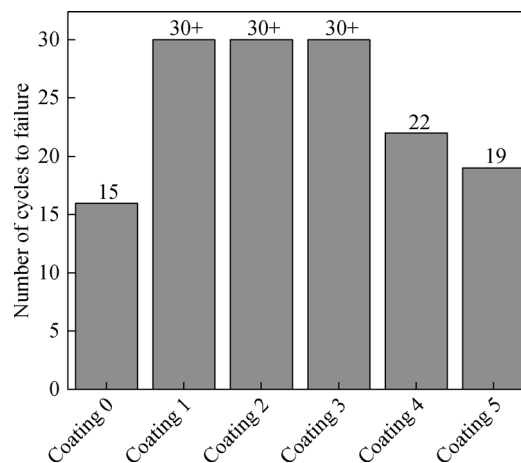


**Fig. 8** Thermal shock test results of coatings

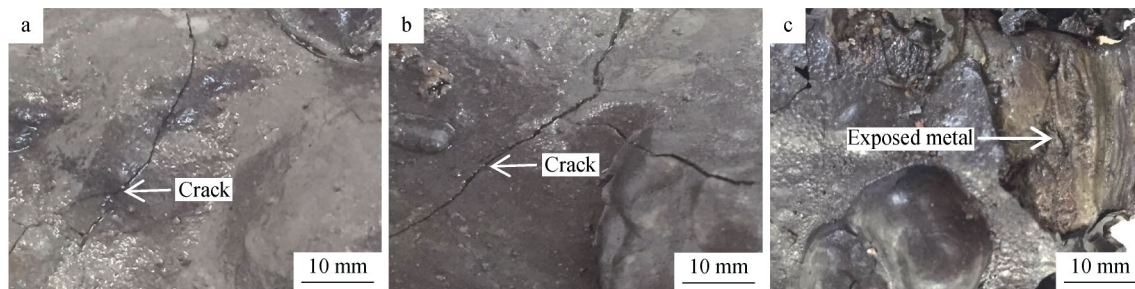


**Fig. 9** Digital images of crack propagation in coating 0 during thermal shock testing after 3 cycles, 7 cycles and 15 cycles

cracks and propagate the cracks when the thermal cycles of the sample are repeated [25]. The duration of thermal cycles of the coating mainly depends on the bond quality between the coating and substrate. From Figs. 4 and 6, some cracks can be observed in coatings 0, 4 and 5 at the area of the interface before the thermal shock testing. These cracks will be propagated easily and lead to poor thermal shock resistance of the coatings. Although coating 1 has some mini cracks also, it has a better thermal resistance than coatings 0, 4 and 5. When Fe addition is 10 wt%–30 wt%, the coating does not peel off the substrate after 30 cycles and it has the best performance of thermal resistance.

For the same kind of coating, generally, the better the bonding quality is between the coating and the substrate, the more the thermal shock cycles last when the coating peels off. Combining the thermal shock test results of Fig. 8 with Figs. 4 and 6, it can be concluded that the coating added 20 wt%–30 wt% Fe has the best binding quality.

### 3.4 Compactness of coating

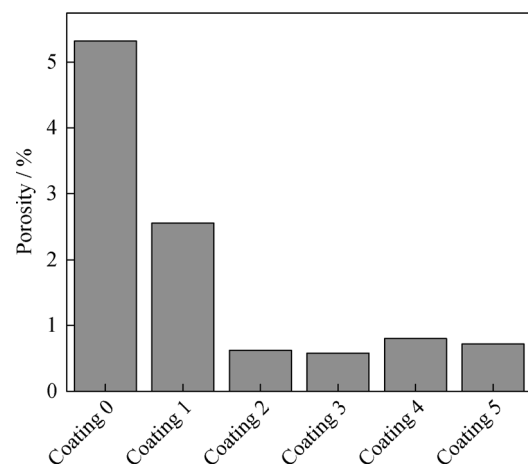
SHS ceramic coating is usually used in the application of abrasive resistance and corrosion resistance [26]. Therefore, compactness is an important criterion of the quality. But as known, the pores and cracks appear commonly. There are two kinds of common pores in the coating [27]. One is shrinkage porosity which is formed during the solidification when some areas of the coating cannot get liquid to fill the shrinkage. Another is gas holes, when the gas cannot escape from the coating during the solidification. There are two main sources of gas, one is the gas primarily existing in the powder mixture, second is the vaporization gas of some materials in the pre-coated mixture because the reaction temperature is extremely high.

Figure 10 shows porosity in the coatings. With the increase in Fe addition to the pre-coated layer, the porosity of the coatings reduces dramatically. When Fe addition is more than 20 wt%, the porosity is less than 1%. When 30 wt% Fe is added to the pre-coated layer, the coating has

the lowest porosity of 0.58%. On the one hand, low Fe addition added to the pre-coated layer can get a high reaction temperature. It can prolong the liquid residence time, and it is beneficial to the escape of gas from the coating. But on the other hand, excessive high temperature can make some materials to be vaporized and a large amount of gas is produced. When the gas does not escape on time from the liquid during the solidification, it will produce the porosity in the coating. The low reaction temperature generates less gas. But if the reaction temperature is too low, the liquid residence time will be too short. The shrinkage of the coating will be not filled from liquid and result in the porosity in the coating. In the respect of the porosity, the coating added 30 wt% Fe to the pre-coated layer has a proper reaction temperature.

### 3.5 Abrasive resistance of coating

According to the above test results, coating 3 has the best bond quality and the lowest porosity. So coating 3 was selected to have a wear test, and the transition layer and mild steel Q235 were also tested for comparison. Figure 11 is the result of abrasive resistance test. The working layer has the best abrasive resistance, and the steel substrate has the worst abrasive resistance. Compared with that of steel



**Fig. 10** Porosity of composite coatings

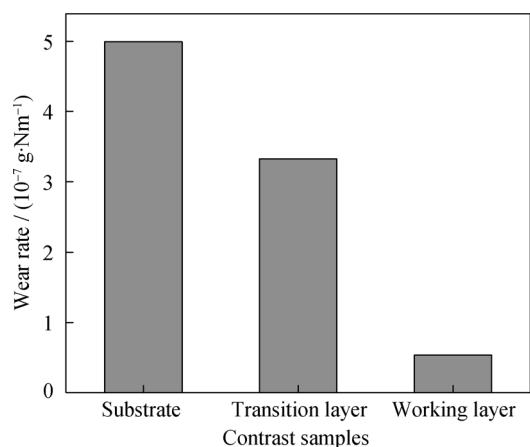


**Fig. 11** Wear rate of samples

substrate, the wear rate of transition layer decreases by 33.4% and the working layer is only about 1/10 that of the substrate.

The microstructure and its phases of coating 3 were checked, and the results are shown in Figs. 12 and 13. Figure 12a gives XRD pattern of transition layer of coating 3, and Fig. 12b shows its microstructure. There are a lot of

small deep gray particles distributed in the light gray structure. Table 5 lists EDS analysis results of point A (at the area of deep gray particles) and point B (at the area of light gray structure) in Fig. 12b. Point A contains 44.15 at% Ti, 38.96 at% C, 11.15 at% iron and 5.74 at% Cr. Point B contains 48.61 at% Fe, 26.34 at% Cr, 21.49 at% C, 2.58 at% Ni and 0.98 at% Ti. Combining XRD and EDS analysis results, it can be concluded that deep gray structure at point A and light gray structure at point B are TiC and Fe(Cr, Ni) solution, respectively. TiC particles disperse in Fe(Cr, Ni) solution, and they improve the abrasive resistance of the transition layer [28–30].

Figure 13a gives XRD pattern of the working layer of coating 3, and it shows that the working layer is composed of  $\alpha$ (Fe, Cr) solution and  $\text{Al}(\text{Cr})_2\text{O}_3$  phase. Figure 13b shows its microstructure, and it reflects that the working layer of coating 3 has granular grains in deep gray and net boundary in light gray, and it is much different from that of the transition layer. Table 5 also lists EDS analysis results of point C (grain particles) and point D (grain boundary) in Fig. 13b. Point C contains 43.13 at% Al, 54.07 at% O, and 2.80 at% Cr. Point D contains 33.78 at% Al, 52.49 at% O, 3.80 at% Cr, 6.25 at% Fe and 3.68 at% C. Combining

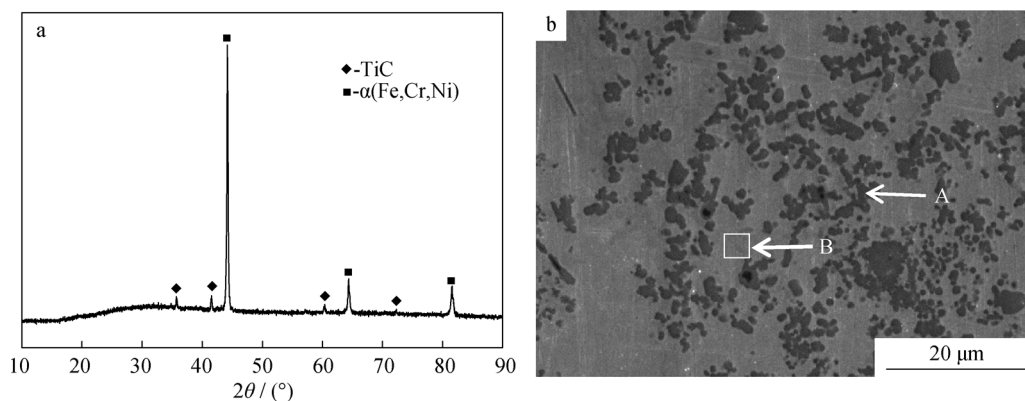


**Fig. 12** a XRD pattern and b microstructure of transition layer of coating 3

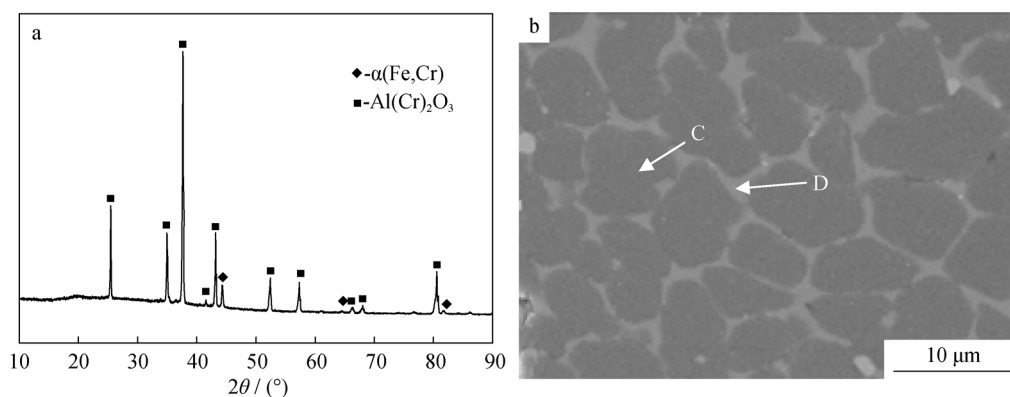


**Fig. 13** a XRD pattern and b microstructure of working layer of coating 3

**Table 5** EDS results of points A, B, C and D in Figs. 12b and 13b (at%)

Locations	C	Ti	Fe	Cr	Ni
A	38.96	44.15	11.15	5.74	0
B	21.49	0.98	48.61	26.34	2.58
Locations	Al	O	Cr	Fe	C
C	43.13	54.07	2.80	0	0
D	33.78	52.49	3.80	6.25	3.68

XRD and EDS analysis results shown in Fig. 13 and Table 5, it can be concluded that deep gray grains are Al(Cr)<sub>2</sub>O<sub>3</sub> and light gray net boundaries are α-Fe(Cr) solution and Al(Cr)<sub>2</sub>O<sub>3</sub>. Al<sub>2</sub>O<sub>3</sub> grains contain a small amount of Cr in solution. Since Al<sub>2</sub>O<sub>3</sub> phase has an extreme high hardness and there are so many Al<sub>2</sub>O<sub>3</sub> phases distributed in working layer, the working layer exhibits a highly abrasive resistance.

#### 4 Conclusion

Al<sub>2</sub>O<sub>3</sub> composite coating manufactured by SHS process was studied. Addition of Fe powders to the pre-coated materials affects the quality of the coating. When 30 wt% Fe is added to the pre-coated transition layer, the coating has a good bond with steel substrate, lower porosity and the best performance of thermal resistance. The mass loss of transition layer is about 1/3 that of the mild steel substrate, and the working layer is about 1/10 that of the substrate, indicating the excellent wear resistance of the composite coating.

**Acknowledgements** This study was financially supported by the National Natural Science Foundation of China (No. 51379070) and the Fundamental Research Funds for the Central Universities (No. 2017B40314).

#### References

- [1] Kubota A, Tsubota Y, Nakano H. Electrodeposition behavior and wear resistance of Co–Ni alloys from sulfamate baths for continuous steel casting mold. *Tetsu to Hagane*. 1999;85(10):728.
- [2] Allcock BW, Lavin PA. Novel composite coating technology in primary and conversion industry applications. *Surf Coat Technol*. 2003;163(2):62.
- [3] Yang Y, Yan DR, Dong YC. Nanostructured ceramic composite coating prepared by reactive plasma spraying micro-sized Al–Fe<sub>2</sub>O<sub>3</sub> composite powders. *J Alloys Compd*. 2011;509(5):L90.
- [4] Hou QY. Microstructure and wear resistance of steel matrix composite coating reinforced by multiple ceramic particulates

- using SHS reaction of Al–TiO<sub>2</sub>–B<sub>2</sub>O<sub>3</sub> system during plasma transferred arc overlay welding. *Surf Coat Technol*. 2013;226(8):113.
- [5] Sharifitabar M, Khaki JV, Sabzevar MH. Microstructure and wear resistance of in situ TiC–Al<sub>2</sub>O<sub>3</sub> particles reinforced Fe-based coatings produced by gas tungsten arc cladding. *Surf Coat Technol*. 2016;285:47.
- [6] Duan XX, Gao SY, Dong Q. Reinforcement mechanism and wear resistance of Al<sub>2</sub>O<sub>3</sub>/Fe–Cr–Mo steel composite coating produced by laser cladding. *Surf Coat Technol*. 2016;291:230.
- [7] Li J, Yu ZH, Wang HP, Li MP. Microstructural characterization of titanium matrix composite coatings reinforced by in situ synthesized TiB + TiC fabricated on Ti6Al4V by laser cladding. *Rare Metals*. 2010;29(5):465.
- [8] Yang K, Rong J, Feng JW. In-situ fabrication of amorphous/eutectic Al<sub>2</sub>O<sub>3</sub>–YAG ceramic composite coating via atmospheric plasma spraying. *J Eur Ceram Soc*. 2016;36(16):4261.
- [9] Xu JY, Zou BL, Tao SY. Fabrication and properties of Al<sub>2</sub>O<sub>3</sub>–TiB<sub>2</sub>–TiC/Al metal matrix composite coatings by atmospheric plasma spraying of SHS powders. *J Alloys Compd*. 2016;672:251.
- [10] Peng YD, Yi Y, Li LY. Iron-based soft magnetic composites with Al<sub>2</sub>O<sub>3</sub>, insulation coating produced using sol–gel method. *Mater Des*. 2016;109:390.
- [11] Tiwari SK, Sahu RK, Pramanick AK. Development of conversion coating on mild steel prior to sol gel nanostructured Al<sub>2</sub>O<sub>3</sub> coating for enhancement of corrosion resistance. *Surf Coat Technol*. 2011;205(21–22):4960.
- [12] La PQ, Bai MW, Xue QJ. A study of Ni<sub>3</sub>Al coating on carbon steel surface via the SHS casting route. *Surf Coat Technol*. 1999;113(1–2):44.
- [13] Morsi K. The diversity of combustion synthesis processing: a review. *J Mater Sci*. 2012;47(1):68.
- [14] Zaitsev AA, Sentyurina ZA, Levashov EA. Structure and properties of NiAl–Cr(Co, Hf) alloys prepared by centrifugal SHS casting. Part 1—room temperature investigations. *Mater Sci Eng A*. 2017;690:463.
- [15] Wang YF, Yang ZG. Finite element analysis of residual thermal stress in ceramic-lined composite pipe prepared by centrifugal-SHS. *Mater Sci Eng A*. 2007;460(1):130.
- [16] Du ZZ, Fu HG, Fu HF. A study of ceramic-lined compound copper pipe produced by SHS-centrifugal casting. *Mater Lett*. 2005;59(14):1853.
- [17] Yuan XY, Liu GH, Jin HB. In situ synthesis of TiC reinforced metal matrix composite (MMC) coating by self propagating high temperature synthesis (SHS). *J Alloys Compd*. 2011;509(30):L301.
- [18] Wang CH, Wang ZH, Zhou ZH, Jiang SQ, Xue XF, Yao JJ. Fabrication and characterization of Al<sub>2</sub>O<sub>3</sub>–metal composite coating on steel plate with non-pressure combustion synthesis. *Rare Metals*. 2013;32(4):390.
- [19] Xue XF, Wang ZH, Zhou ZH. Bonding characteristics of the Al<sub>2</sub>O<sub>3</sub>–metal composite coating fabricated onto carbon steel by combustion synthesis. *Int J Miner Metal Mater*. 2014;44(9):886.
- [20] Masanta M, Shariff SM, Choudhury AR. Microstructure and properties of TiB<sub>2</sub>–TiC–Al<sub>2</sub>O<sub>3</sub> coating prepared by laser assisted SHS and subsequent cladding with micro-/nano-TiO<sub>2</sub>, as precursor constituent. *Mater Des*. 2015;90:307.
- [21] Masanta M, Shariff SM, Choudhury AR. Tribological behavior of TiB<sub>2</sub>–TiC–Al<sub>2</sub>O<sub>3</sub> composite coating synthesized by combined SHS and laser technology. *Surf Coat Technol*. 2010;204(16):2527.
- [22] Zang CC, Wang YZ, Zhang YD, Zhang YD, Li JH, Zeng H, Zhang DQ. Microstructure and wear-resistant properties of NiCr–Cr<sub>3</sub>C<sub>2</sub> coating with Ni45 transition layer produced by laser cladding. *Rare Metals*. 2015;34(7):491.



- [23] Almagour B, Grzesiak D, Jen MY. Selective laser melting of TiC reinforced 316L stainless steel matrix nanocomposites: Influence of starting TiC particle size and volume content. *Mater Des.* 2016;104:141.
- [24] Qian J, Zhang J, Li S. Study on laser cladding NiAl/Al<sub>2</sub>O<sub>3</sub> coating on magnesium alloy. *Rare Metal Mater Eng.* 2013;42(3):466.
- [25] Si TZ, Liu N, Zhang QA. Thermal shock fatigue behavior of TiC/Al<sub>2</sub>O<sub>3</sub> composite ceramics. *Rare Metals.* 2008;27(3):308.
- [26] Mahmoodian R, Hassan MA, Hamdi M. In-situ TiC-Fe-Al<sub>2</sub>O<sub>3</sub>-TiAl/Ti<sub>3</sub>Al composite coating processing using centrifugal assisted combustion synthesis. *Compos Part B Eng.* 2014;59(3):279.
- [27] Sierra C, Vázquez AJ. NiAl coating on carbon steel with an intermediate Ni gradient layer. *Surf Coat Technol.* 2006;200(14–15):4383.
- [28] Jones M, Horlock AJ, Shipway PH. Microstructure and abrasive wear behavior of FeCr-TiC coatings deposited by HVOF spraying of SHS powders. *Wear.* 2001;249(s3–4):246.
- [29] Tan YF, Long HE, Wang XL. Tribological properties and wear prediction model of TiC particles reinforced Ni-base alloy composite coatings. *Trans Nonferrous Met Soc China.* 2014;24(8):2566.
- [30] Akhtar F, Guo SJ, Feng PZ. TiC-Maraging stainless steel composite: microstructure, mechanical and wear properties. *Rare Metals.* 2006;25(6):630.